Scientific Paper / Artículo Científico

UNIVERSIDAD POLITÉCNICA SALESIANA ECUADOR
INGENIUS
Revista de Ciencia y Tecnología
https://doi.org/10.17163/ings.n30.2023.03
pISSN: 1390-650X / eISSN: 1390-860X

Polynomial cross-roots application for the exchange of radiant energy between two triangular geometries

Aplicación de raíces cruzadas polinomiales al intercambio de energía radiante entre dos geometrías triangulares

Yanan Camaraza-Medina[1,*]

Received: 12-02-2023, Received after review: 21-04-2023, Accepted: 26-04-2023, Published: 01-07-2023

Abstract

The view factor between surfaces is essential in radiative heat transfer. Currently, there are no analytical solutions to evaluate the view factors between triangular geometries with common edges and angle θ due to the high mathematical complexity associated with their development. For these configurations, the literature only has Sauer's graphical solutions, which generate average errors of 12%. This study developed an approximate method that does not involve high mathematical complexity and guarantees a fit of less than 12%. For this purpose, 32 different geometric configurations were studied (8 basic and 24 derived), obtaining the solutions for each evaluated case. 42 different transmitter and receiver dimensions were used to validate the models obtained. The vision factors were computed in each case using the analytical solution (AS), the numerical solution obtained with Simpson's 1/3 multiple rules (SMR) with five intervals, and Bretzhtsov's cross-root (BCR). The results obtained in each of the eight base cases were compared. In all cases evaluated, the BCR showed the best fits with an error of ±6% in more than 90% of the samples, while the SMR showed an average scatter of ±6% in 65% of the data. The practical nature of the contribution and the reasonable fitting values obtained show that this proposal is a suitable tool for thermal engineering.

Keywords: triangular surfaces, Bretzhtsov cross-root, view factor

Resumen

El factor de visión entre superficies es esencial en la transferencia de calor por radiación. En la actualidad, para evaluar los factores de visión entre geometrías triangulares con bordes comunes y ángulo θ no se dispone de soluciones analíticas, debido a la elevada complejidad matemática asociada a su desarrollo. Para estas configuraciones, la literatura solo tiene las soluciones gráficas de Sauer, cuyo uso genera errores medios del 12 %. En este trabajo se desarrolla un método aproximado que no genere una alta complejidad matemática y que garantice un ajuste inferior al 12 %. Para este propósito fueron estudiadas 32 configuraciones geométricas diferentes (8 básicas y 24 derivadas), siendo obtenidas las soluciones para cada uno de los casos evaluados. Para la validación de los modelos obtenidos se usaron 42 dimensiones diferentes de emisor y receptor, siendo computados en cada caso los factores de visión mediante la solución analítica (SA), la solución numérica obtenida con la regla múltiple de Simpson 1/3 (RMS) con cinco intervalos y mediante la raíz cruzada de Bretzhtsov (RCB), comparándose finalmente los resultados obtenidos en cada uno los ocho casos básicos. En todos los casos evaluados, la RCB mostró los mejores ajustes, con un error de ±6 % en más del 90 % de las muestras, mientras que la RMS mostró una dispersión media de ±6 % en el 65 % de los datos. La naturaleza práctica de la contribución y los valores razonables de ajuste obtenidos, establecen a la propuesta como una herramienta adecuada para su uso en la ingeniería térmica.

Palabras clave: superficies triangulares, raíz cruzada de Bretzhtsov, factor de visión

[1,*]Technical Sciences Faculty, University of Matanzas, Cuba. Corresponding author ✉: yanan.camaraza@umcc.cu.

Suggested citation: Camaraza-Medina, Y. "Polynomial cross-roots application for the exchange of radiant energy between two triangular geometries," *Ingenius, Revista de Ciencia y Tecnología*, N.° 30, pp. 29-41, 2023, DOI: https://doi.org/10.17163/ings.n30.2023.03.

1. Introduction

It is required to evaluate the thermal radiation between surfaces in thermal engineering. The vision factor establishes what fraction of the radiant energy emitted by one surface is intercepted by another [1].

The geometrical relationship between two surfaces and its influence on the view factor has been studied for decades, obtaining numerical and analytical solutions for different geometrical configurations [2–5]. For example, Howell extensively compiled view factors with more than 320 different configurations [6].

The accelerated leap in using computational techniques has generalized the implementation of commercial programs based on the finite element method (FEM) to solve thermal radiation problems [7–10].

Three-dimensional edge problems are reduced to surfaces with common edges and angle θ included. However, shape factor algebra is tedious for these geometries, so numerical solutions such as FEM are preferred [11–13].

In FEM, meshes generally use triangular elements and rarely use rectangles or squares unless the overall geometry is a perfect cube. Determining an analytical solution for the view factor between triangular geometries requires sums of multiple integrals due to changing integration contours. In many cases, the solutions are not elementary functions, requiring the manipulation of inverse trigonometric functions, polylogarithms, and sums of infinite series [14].

This makes direct integration extremely tedious for unshared or without common edges geometries, so numerical integration is preferred. For this reason, analytical solutions for these types of geometries are lacking [15].

Using SMR with five intervals, the view factors were plotted for several perpendicular triangular geometries with common edges [16]. However, their graphical interpretation generated mean errors of 12 %, demonstrating that they do not apply to FEM since they cannot be discretized. In the specialized technical literature, only this graphical solution is available to obtain the view factors between triangular geometries [6–13].

The BCR method provides a proper fit during the approximation of complex functions, so it can be used to create the expressions required in the FEM discretization. The BCR method is similar to the FEM because its mathematical conception is based on the formation of nodes, obtaining the polynomial fits from the interconnection of the nodes [17]. Considering the above, it is demonstrated that there is a lack of analytical solutions (exact or approximate) to estimate the view factors between triangular geometries with common edges and angle θ included.

Therefore, this study aims to develop approximate solutions to calculate the view factors between triangular geometries with common edges and angle θ included, without involving high mathematical complexity and guaranteeing a good fit concerning the SA. Thus, it is possible to establish a new analysis method for use in the FEM.

This research develops the exact analytical solutions for eight basic triangular geometries and their respective BCRs. For comparison, 42 examples with various aspect ratios were calculated for each geometry, using the AS, BCR, and SMR.

The practical nature of the contribution and the reasonable fitting values obtained demonstrate that this proposal is a suitable tool to be applied in thermal engineering and related practices that require thermal radiation calculations between triangular geometries.

2. Materials y methods

2.1. Definition of the view factor

The view factor F_{12} depends on the position and geometrical configuration of the emitting surface A_1 and the receiving surface A_2, defined as the fraction of the radiation leaving the former and intercepted by the latter, which is expressed as [18], in equation (1).

$$F_{12} = \frac{1}{\pi A_1} \int_{A_1} \int_{A_2} \frac{cos\ O_1\ cos\ O_2}{r^2}\ dA_2\ dA_1 \qquad (1)$$

Where: O_1, O_2- angles between the normal vector of the areas dA_1 and dA_2 and the line connecting the center of the surfaces A_1 and A_2, respectively. $r-$ distance between the centers of surfaces A_1 and A_2, (see Figure 1).

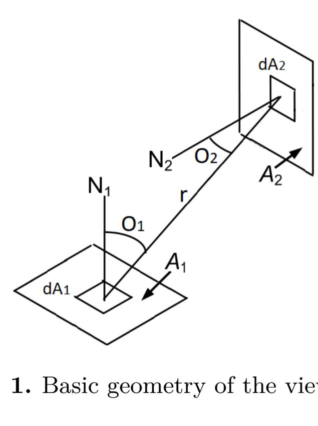

Figure 1. Basic geometry of the view factor

Equation (1) requires a double integration over the surfaces, which is complex and time-consuming since a large set of immediate integrals must be manipulated and subsequently factorized.

Numerical approximations can simplify the analysis because a suitable fit can be obtained with an appropriate set of intervals. For three-dimensional (3-D) configurations, various solution methods, such as contour integration, are available [19–24].

This work uses contour integration to obtain the view factor of the eight geometries analyzed. To approximate the special functions generated in the integration, the BCR method is used.

2.2. Mesh creation for surface elements

In modern engineering, triangular elements are widely used to generate meshes. In contrast, rectangular or square elements are rarely used, except in cases where the overall geometry is a perfect cube. Formulating this type of geometry requires a complex mathematical treatment that includes sums of the quadruple integral equation (1) caused by the variation of the limits in the projection on each coordinate axis. The viewing factor between two rectangular surfaces of the same width, with common edge and angle θ included, is given by equation (2) (see Figure 2).

$$f_{(1)} = F_{a-b} = \frac{sin^2\theta}{\pi A_1}\int_0^L dy_1 \int_0^D dx \int_0^W dz \int_0^D \frac{xz}{\left\{(y_1-y_2)^2+x^2+z^2-2xzcos\ \theta\right\}^2}\, dy_2 \qquad (2)$$

The following substitutions are used to evaluate equation (2).

$$X = W/D; Y = L/D; R = \sqrt{X^2+Y^2-2XYcos\ \theta} \qquad (3)$$

After evaluating equation (2), we obtain the following solution $f_{(1)}$, (equation (4)).

$$f_{(1)} = \frac{1}{\pi Y}\left\{\begin{array}{c} -\frac{sin\ 2\theta}{4}\left\{Y^2 tan^{-1}\left(\frac{X}{Y}csc\ \theta - cot\ \theta\right) + X^2 tan^{-1}\left(\frac{Y}{X}csc\ \theta - cot\ \theta\right) + XY sin\ \theta + \left(\frac{\pi}{2}-\theta\right)\left(X^2+Y^2\right)\right\} + \\ +\frac{1}{4}ln\left\{\left\{\frac{X^2}{R^2}\left(\frac{1+X^2}{1+R^2}\right)^{cos\ 2\theta}\right\}^{X^2 sin^2\ \theta}\left(\frac{Y^2+Y^2R^2}{R^2+Y^2R^2}\right)^{Y^2 sin^2\ 2\theta}\left(\frac{(1+X^2)(1+Y^2)}{1+R^2}\right)^{cos^2\ \theta+1}\right\} + \\ +(sin^3\ \theta\ cos\ \theta)tan^{-1}\left(\frac{Y sin\ \theta\sqrt{X^2+cot^2\ \theta+1}}{X^2-YXcos\ \theta+1}\right)\sqrt{X^4+X^2(cot^2\ \theta+1)} + Xtan^{-1}\left(\frac{1}{X}\right) + \\ +Ytan^{-1}\left(\frac{1}{Y}\right) - Rcot^{-1}(R) + \frac{sin\ 2\theta}{2}\int_0^Y \sqrt{Z^2+cot^2\ \theta+1}\ tan^{-1}\left(\frac{Xsin\ \theta\sqrt{z^2+cot^2\ \theta+1}}{z^2-zXcos\ \theta}+1\right)dz \end{array}\right\} \qquad (4)$$

In equations (2), (3) and (4), the angle θ is given in radians. Equation (4) is very complex; for this reason, the last integral was not solved because its solution can be obtained numerically using Simpson's 1/3 rule (with at least eight intervals).

Drawing diagonal lines divides the emitting surface A_1 and receiving surface A_2 into eight triangular geometries. Applying the shape algebra for the geometry in Figure 3, $\frac{1}{2}n^{n-1} = \frac{1}{2}4^{4-1} = 32$ combinations of view factors are obtained (see Figure 3). The analyzed geometry is symmetric; therefore, it is possible to define seven basic cases, as shown in Figure 4.

Case 1: Right triangle to rectangle, with common side and angle θ between both surfaces.

Case 2: Right triangle to right triangle, with common side and angle θ between both surfaces: vertices at a common point.

Case 3: Right triangle to right triangle, with common side and angle θ between both surfaces: vertices at opposite ends.

Case 4: Isosceles triangle to rectangle, with common side and angle θ between both surfaces.

Case 5: Right triangle to right triangle of different size, with angle θ between both surfaces: vertices at a common point.

Case 6: Right triangle to right triangle of different size, with angle θ between both surfaces: vertices at opposite ends.

Case 7: Perpendicular right triangles with an equal edge and arranged in opposite directions.

The view factors for the remaining cases can be obtained using the sum rule.

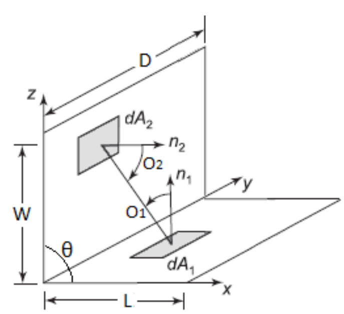

Figure 2. Rectangles of equal width, with common edge and angle θ included

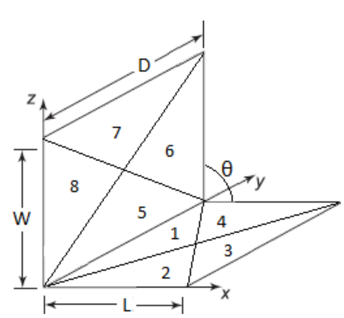

Figure 3. Division of rectangular surfaces into triangular elements

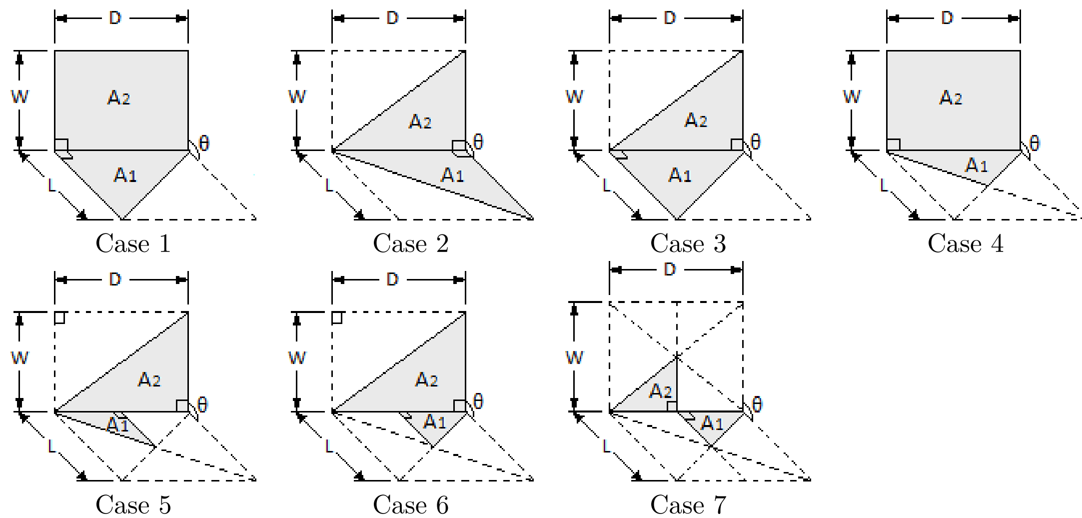

Figure 4. Basic configurations for triangular geometries

2.3. Modeling of the view factor. Case 1

In Case 1 (see Figure 5), it is satisfied that the equation (5).

$$\cos O_1 = \frac{z\sin\,\theta}{r};\cos O_2 = \frac{x\sin\,\theta}{r} \\ r = (y_1 - y_1)^2 + x^2 + z^2 - 2xz\cos\,\theta \tag{5}$$

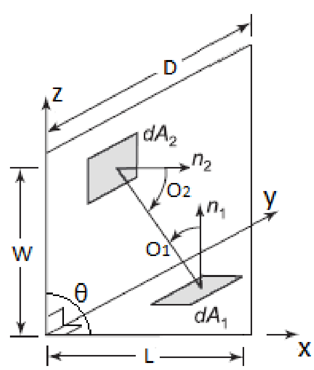

Figure 5. Basic Geometry for Case 1

Substituting equation (5) in equation (1), the view factor F_{12} is given by equation (6).

$$f_2 = \frac{\sin^2\,\theta}{\pi A_1}\int_0^L dy_1 \int_0^{y_{1D/L}} dx \int_0^D dz \cdot \\ \cdot \int_0^W \frac{xz}{\left\{(y_1-y_2)^2+x^2+z^2-2xz\cos\,\theta\right\}^2} dy_2 \tag{6}$$

In equation (6), the change indicated in equation (7) was made to perform the integration.

$$W = a; D = b; L = c \tag{7}$$

Equation (6) is first integrated on the emitting surface A_1, obtaining a sum of integrals, which is given by equation (8).

After a complex process in which it was necessary to solve $n^n = 4^4 = 256$ primitive functions, the sum of double integrals of equation (8) was solved, whose solution is given in equation (9).

$$f_2 = \frac{1}{\pi A_1}\int_0^b dy \int_0^c \left\{ \tan^{-1}\left(\frac{1}{z}\right) + \frac{z\sin^2\,\theta}{2} \ln\left[\frac{z^2\left(z^2-2az\cos\,\theta+1+a^2\right)}{\left(1+z^2\right)\left(a^2+z^2-2az\cos\,\theta\right)}\right] - z\sin\,\theta\cos\,\theta\left[\frac{\pi}{2} - \theta + \tan^{-1}\left(\frac{a-z\cos\,\theta}{z\sin\,\theta}\right)\right] + \right. \\ \left. + \cos\,\theta\sqrt{1+z^2\sin^2\,\theta}\left[\tan^{-1}\left(\frac{a-z\cos\,\theta}{\sqrt{1+z^2\sin^2\,\theta}}\right) + \tan^{-1}\left(\frac{z\cos\,\theta}{\sqrt{1+z^2\sin^2\,\theta}}\right)\right] + \frac{a\cos\,\theta - z}{\sqrt{a^2+z^2-2az\cos\,\theta}}\tan^{-1}\left(\frac{1}{\sqrt{a^2+z^2-2az\cos\,\theta}}\right)\right\} dz \tag{8}$$

$$f_{(2)} = 2f_{(1)}\left\{ \frac{a^2b^2}{8\left(a^2+b^2\right)}\ln\left(\frac{b^2+c^2}{\left(a^2+c^2\right)^2}\right) + \frac{a^2b^4}{4\left(a^2+b^2\right)^2}\ln\left(\frac{b\left(a^2+c^2\right)}{a\left(b^2+c^2\right)}\right) + \frac{a^4b^2}{4\left(a^2+b^2\right)^2}\ln\left(\frac{b}{a}\right) + \frac{a^2c^2}{8\left(a^2+b^2\right)}\ln\left(\frac{\left(b^2+c^2\right)\left(a^2+b^2+c^2\right)}{c^2\left(a^2+c^2\right)}\right) + \right. \\ + \frac{a^2}{8}\ln\left(\frac{a^4\left(a^2+b^2+c^2\right)^2}{\left(a^2+b^2\right)^2\left(a^2+c^2\right)}\right) + \frac{b^2}{8}\ln\left(\frac{\left(a^2+b^2\right)\left(a^2+c^2\right)}{b^2\left(a^2+b^2+c^2\right)}\right) + \frac{c^2}{8}\ln\left(\frac{c^2\left(a^2+b^2+c^2\right)}{\left(a^2+b^2\right)\left(a^2+c^2\right)}\right) + \frac{3}{4}ab\,\tan^{-1}\left(\frac{b}{a}\right) + \frac{1}{2}bc\,\tan^{-1} \\ -\frac{1}{2}b\sqrt{a^2+c^2}\tan^{-1}\left(\frac{b}{\sqrt{a^2+c^2}}\right) - \frac{a^4}{8\left(a^2+b^2\right)}\ln\left(a^2+c^2\right) + \frac{ab^2(2a-\pi b)}{8\left(a^2+b^2\right)} + \\ + \frac{a^2b^2\left(\frac{b^4}{a^2+b^2} - b^2 - c^2\right)}{2\left(a^2+b^2\right)^{\frac{3}{2}}\sqrt{b^2+c^2-\frac{b^4}{a^2+b^2}}}\tan^{-1}\left(\frac{\left(a^2+b^2\right)^{\frac{3}{2}}\sqrt{b^2+c^2-\frac{b^4}{a^2+b^2}}}{\left(a^2+b^2\right)^{\frac{3}{2}}\left(b^2+c^2-\frac{b^4}{a^2+b^2} - b^2\left\{\left(a^2+b^2\right)-b^2\right\}\right)}\right) - \\ \left. -\frac{1}{2}\int_0^a\left[\frac{bx^2}{a\sqrt{x^2+c}}\tan^{-1}\left(\frac{a\sqrt{x^2+c}}{x^2+c^2+\frac{b^2}{a^2}\left(x^2-ax\right)}\right) + \frac{bx}{\sqrt{x^2+c}}\tan^{-1}\left(\frac{\frac{b}{a}x-b}{\sqrt{x^2+c}}\right)\right]\right\} dx \tag{9}$$

In equation (9), the term $f_{(1)}$ is obtained by equation (4). Due to the complexity of equation (9), the last integral is not solved, and its solution is obtained numerically using the SMR (twelve intervals are recommended). Equation (9) is transformed as the equation (10).

$$F_{12} = f_{(n)} = 2F_{(1)} \cdot \varphi n \tag{10}$$

Equation (10) is then transformed by dividing each dimensional variable by the length of the common edge b. The result is shown below the equation (11).

$$\begin{gathered} 1 = b/b; X = a/b; Y = c/b \\ R = \sqrt{X^2 + Y^2 - 2XY\cos\theta} \end{gathered} \tag{11}$$

Applying in equation (9) the change of variables of equation (11), the analytical solution for Case 1 is obtained, which is given by equation (12).

$$\begin{aligned} f_{(2)} = 2f_{(1)} \Bigg\{ & \tfrac{X^2}{8\left(X^2+1\right)} ln\left(\tfrac{Y^2+1}{R^4}\right) + \tfrac{X^2}{4\left(X^2+1\right)^2} ln\left(\tfrac{R^2}{X\left(Y^2+1\right)}\right) + \tfrac{X^2Y^2}{8\left(X^2+1\right)} ln\left(\tfrac{\left(Y^2+1\right)\left(R^2+1\right)}{Y^2R^2}\right) + \\ & + \tfrac{X^4}{4\left(X^2+1\right)^2} ln\left(\tfrac{1}{X}\right) - \tfrac{X^4}{8\left(X^2+1\right)} ln\left(R^2\right) + \tfrac{3X}{4} tan^{-1}\left(\tfrac{1}{X}\right) + \tfrac{Y}{2} tan^{-1}\left(\tfrac{1}{Y}\right) - \tfrac{R}{2} tan^{-1}\left(\tfrac{1}{R}\right) + \\ & + \tfrac{1}{8} ln\left\{\left(\tfrac{X^4\left(R^2+1\right)^2}{R^2\left(X^2+1\right)^2}\right)^{X^2} \left(\tfrac{Y^2\left(R^2+1\right)}{R^2\left(X^2+1\right)}\right)^{Y^2} \left(\tfrac{R^2\left(X^2+1\right)}{R^2+1}\right)\right\} + \tfrac{2X^2-\pi}{8\left(X^2+1\right)} - \\ & + \frac{X^2\left(Y^2 - \frac{X^2+2}{X^2+1}\right)}{2\left(X^2+1\right)^{\frac{3}{2}}\sqrt{Y^2 - \frac{X^2+2}{X^2-1}}} tan^{-1}\left(\frac{\left(X^2+1\right)^{\frac{3}{2}}\sqrt{Y^2 - \frac{X^2+2}{X^2+1}}}{\left(X^2+1\right)\left(Y^2 - \frac{X^2+2}{X^2+1}\right) - X^2}\right) - \end{aligned} \tag{12}$$

Equation (12) is a combination of variables $(Y; X)$. Evaluating this equation may be difficult because it is necessary to solve polylogarithms, sums of infinite series, and inverse trigonometric functions. However, using Bretzhtsov's cross-root method, it is possible to obtain an approximate result, facilitating the calculation of the view factor.

To implement the cross-root method, nodes are constructed using prefixed values $(Y; X)$, which are joined using diagonal lines forming the families of curves a_n and b_n. In this study, the values $Y = (0.1; 0.2; 0.5; 1; 3; 10)$ and $X = (0.1; 0.3; 0.6; 1; 3; 6; 10)$ are used.

Tables 1 and 2 summarize the combination of variables $(Y; X)$ for each node and the nodes that integrate each curve a_n and b_n, respectively. Figure 6 plots the families of curves a_n and b_n.

The next step is to compute the vision factor using equation (12) for each of the combinations of variables $(Y; X)$ in Table 1, plotting them in a $F_{12}; X$ diagram, as shown in Figure 7. The union of the nodes along the x-axis makes it possible to create a third family of curves c_n. A particularity is that all the nodes integrating the same curve c_n have the same value of the variable Y, as shown in Table 1. Table 3 summarizes the nodes integrating each c_n curve.

Table 1. Combinations of variables $(Y; X)$ for each node

node	(Y, X)	node	(Y, X)	node	(Y, X)	node	(Y, X)
1	3 ; 0.1	12	1 ; 0.6	23	0.5 ; 1	34	0.5 ; 6
2	10 ; 0.3	13	3 ; 1	24	1 ; 3	35	1 ; 10
3	1 ; 0.1	14	10 ; 3	25	3 ; 6	36	0.1 3
4	3 ; 0.3	15	0.1 ; 0.1	26	10 ; 10	37	0.2 ; 6
5	10 ; 0.6	16	0.2 ; 0.3	27	0.1 ; 0.6	38	0.5 ; 10
6	0.5 ; 0.1	17	0.5 ; 0.6	28	0.2 ; 1	39	0.1 ; 6
7	1 ; 0.3	18	1 ; 1	29	0.5 ; 3	40	0.2 ; 10
8	3 ; 0.6	19	3 ; 3	30	1 ; 6	41	10 ; 0.1
9	10 ; 1	20	10 ; 6	31	3 ; 10	42	0.1 ; 10
10	0.2 ; 0.1	21	0.1 ; 0.3	32	0.1 ; 1		
11	0.5 ; 0.3	22	0.2 ; 0.6	33	0.2 ; 3		

Table 2. Nodes integrating each curve a_n and b_n

$\mathbf{a_n}$	**nodes**	$\mathbf{b_n}$	**nodes**
a_1	1-2	b_1	10-21
a_2	3-4-5	b_2	6-16-27
a_3	6-7-8-9	b_3	3-11-22-32
a_4	10-11-12-13-14	b_4	1-7-17-28-36
a_5	15-16-17-18-19-20	b_5	41-4-12-23-33-39
a_6	21-22-23-24-25-26	b_6	2-8-18-29-37-42
a_7	27-28-29-30-31	b_7	5-13-24-34-40
a_8	32-33-34-35	b_8	9-19-30-38
a_9	36-37-38	b_9	14-25-35
a_{10}	39-40	b_{10}	20-31

Table 3. Nodes integrating each c_n curve

$\mathbf{c_n}$	**nodes**	$\mathbf{c_n}$	**nodes**
c_1	15-21-27-32-36-39-42	c_4	3-7-12-18-24-30-35
c_2	10-16-22-28-33-37-40	c_5	1-4-8-13-19-25-31
c_3	6-11-17-2329-34-38	c_6	41-2-5-6-14-20-26

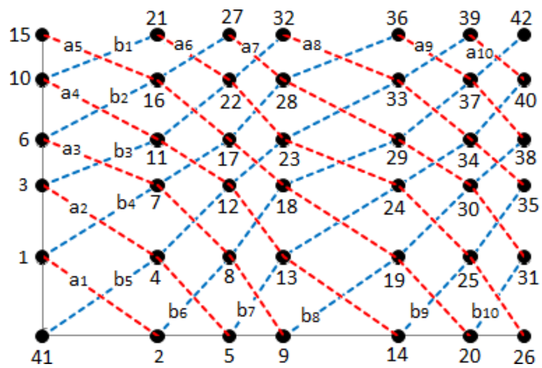

Figure 6. Families of curves a_n and b_n

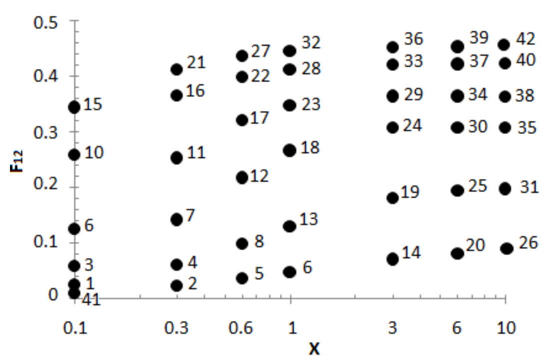

Figure 7. Scheme for applying cross-roots

Each curve of the families a_n, b_n, c_n is approximated individually by the Least Squares Method (LSM), using a third-degree polynomial in the form $mX^3 + nX^2 + oX + p$, thus establishing a dependence between the view factor F_{12} and the X variable. Figure 8 shows the application of the method for curves a_5, b_5, c_4.

Table 4 shows the values of the constants m, n, o, p obtained by applying LMS to all the curves a_n, b_n, c_n. The m, n, o, p values are averaged in each curve, thus obtaining the approximate functions A_n, B_n, C_n.

For each curve, the apparent angle of transmissibility (see Figure 8) is given by the equation (13)

$$\psi = tan^{-1}\left(\frac{X}{Y}\right) \tag{13}$$

Therefore, Bretzhtsov's cross-root is given by the equation (14).

$$\varphi_n = A_n\psi^2 + B_n\psi + C_n \tag{14}$$

Table 4 shows the constants m, n, o, p for the polynomials A_n, B_n, C_n. For the approximations, the X variables were used, keeping the Y variables constant; therefore, to apply the cross roots, the Y variables were alternated by X, obtaining the following equations (15) to (17) for the polynomials A_n, B_n, C_n.

$$A_n = -0.022Y^3 + 0.316Y^2 - 0.89Y + 0.5 \tag{15}$$

$$B_n = 0.056Y^3 - 0.783Y^2 + 2.23Y - 1.43 \tag{16}$$

$$C_n = 0.03Y^3 + 0.407Y^2 - 1.07Y + 2.02 \tag{17}$$

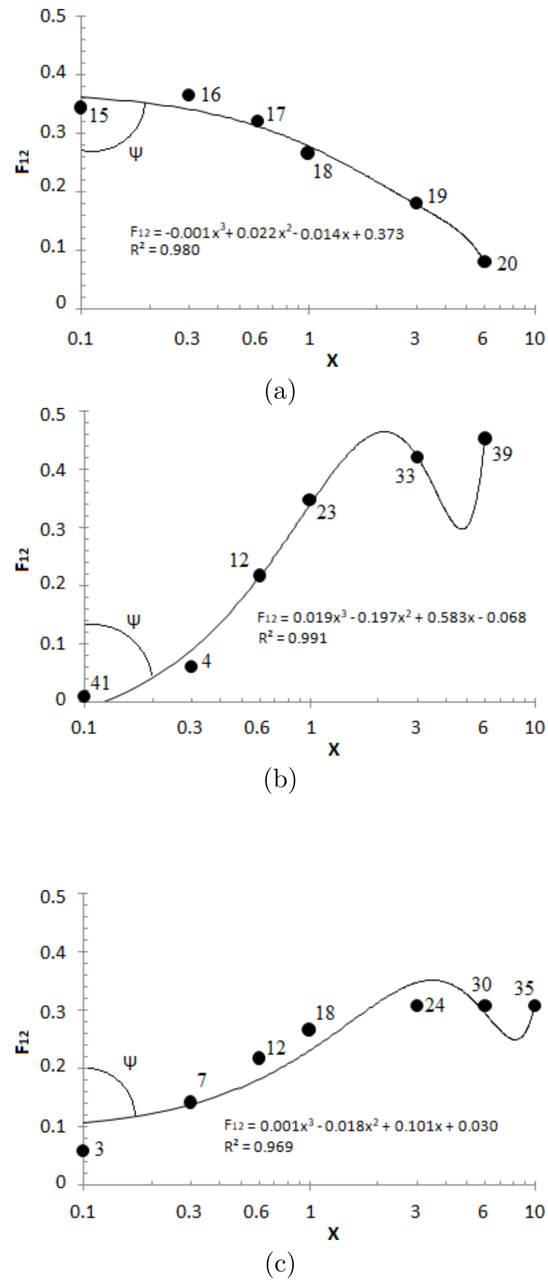

Figure 8. Approximation by Least Squares (a), curve a_5, (b) curve b_5, (c) curve c_4

Substituting equations (15) through (17) into equation (14), we obtain that Bretzhtsov's cross-root for Case 1 is given by equation (18).

$$\varphi_n = \left(-0.022Y^3 + 0.316Y^2 - 0.89Y + 0.5\right)\psi^2 + \left(0.056Y^3 - 0.783Y^2 + 2.23Y - 1.43\right)\psi - \\ -0.03Y^3 + 0.407Y^2 - 1.07Y + 2.02 \tag{18}$$

Table 4. Constants m, n, o, p obtained by applying LMS

Curve	m	n	o	p
a_2	0	0.186	–1.023	0.51
a_3	0.549	0.32	–0.528	0.91
a_4	–0.278	0.28	–0.88	0.352
a_5	–0.337	0.52	–0.514	0.373
a_6	–0.11	0.64	–2.48	0.484
a_7	0	0.66	–0.95	0.456
a_8	0	–0.03	–0.713	0.447
a_9	0	–0.05	–0.03	0.468
average A_n	–0.022	0.316	–0.89	0.5
Curve	**m**	**n**	**o**	**p**
b_1	0	0	3.06	–1.181
b_2	0	–1.96	2.97	–1.53
b_3	0	–1.18	2.34	–1.44
b_4	0.424	–0.592	1.98	–1.67
b_5	0.019	–0.197	2.583	–1.068
b_6	0.106	–1.91	3.22	–2.99
b_7	0.011	–0.75	2.37	–1.07
b_8	0	–0.93	2.29	–1.123
b_9	0	–0.31	1.19	–1.285
b_{10}	0	0	0.29	–0.94
average B_n	0.056	–0.783	2.23	–1.43
Curve	**m**	**n**	**o**	**p**
c_1	0	0.16	–1.69	2.374
c_2	0.018	0.28	–1.103	2.307
c_3	0.02	0.34	–1.161	2.183
c_4	0.002	–0.035	–1.173	2.088
c_5	0.14	0.99	–0.92	2.16
c_6	0	0.71	–0.37	1.01
average C_n	0.03	0.407	–1.07	2.02

Substituting equation (18) in equation (10), the view factor for Case 1 is obtained, which is given by equation (19).

$$f_{(2)} = 2f_{(1)} \cdot \{ \left(-0.022Y^3 + 0.316Y^2 - 0.89Y + 0.5\right)\psi^2 + \left(0.056Y^3 - 0.783Y^2 + 2.23Y - 1.43\right)\psi - \\ -0.03Y^3 + 0.407Y^2 - 1.07Y + 2.02 \} \tag{19}$$

3. Results and discussion

For practical engineering use, equation (19) is much simpler than the analytical solution (SA) of equation (12). The percentage deviation (error) is computed with respect to the analytical solution and is obtained by the following relation in equation (20) [25].

$$D_{\%} = 100 \cdot \frac{SA - Val}{SA} \tag{20}$$

Where: $D_{\%}$ is the percentage of deviation. SA is the view factor obtained by the analytical solution. Val is the view factor obtained by approximate methods.

To calculate the $D_{\%}$ values, the view factors are computed for the 42 combinations of variables $(Y;X)$ in Table 1, using the AS, the SMR with five intervals, and the view factors obtained with the BCR.

Figure 9 plots the $D_{\%}$ values obtained with equation (18) for the view factors calculated by SMR and BCR, adjusted in error bands of ±3% and ±6%.

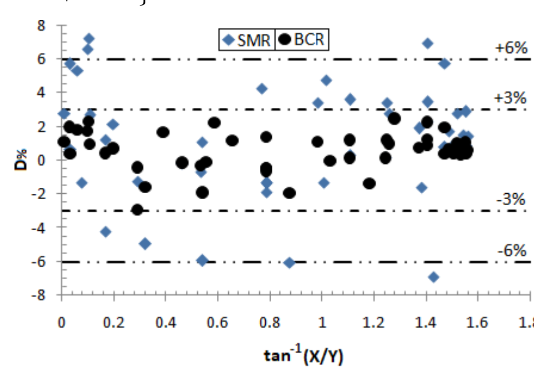

Figure 9. $D_{\%}$ obtained with equation (18) for Case 1

For Case 1, Figure 9 shows that BCRs have a better fit with respect to SA, with a mean error of ±3% for 100% of the $(Y;X)$ points analyzed. On the contrary, the view factors obtained with SMR have a lower fit with respect to the AS, with mean errors of ±3% and ±6% for 54,8% and 85,7% of the $(Y;X)$ points evaluated, respectively.

3.1. Modeling and validation of Cases 2 to 7

For Cases 2 to 7 (see Figure 4), mathematically, the view factor F_{12} is given by equations (21) to (26).

$$Case\ 2 \quad f_{(3)} = \frac{sin^2\theta}{\pi A_1}\int_0^L dy_1 \int_0^{y_1 D/L} dx \int_0^W dy_2 \int_0^{y_2 D/L} \frac{xz}{\{(y_1-y_2)^2+x^2+z^2-2xzcos\theta\}^2} dz \tag{21}$$

$$Case\ 3 \quad f_{(4)} = \frac{sin^2\theta}{\pi A_1} \int_0^{L} dy_1 \int_0^{y_1 D/L} dx \int_0^{W} dy_2 \int_0^{y_2 D/L} \frac{xz}{\{(y_1-y_2)^2+x^2+z^2-2xzcos\theta\}^2} dz \tag{22}$$

$$Case\ 4 \quad f_{(5)} = \frac{sin^2\theta}{\pi A_1} \int_0^{L/2} dy_1 \int_0^{y_1 D/L} dx \int_0^{W} dz \int_0^{y_2 D/L} \frac{xz}{\{(y_1-y_2)^2+x^2+z^2-2xzcos\theta\}^2} dy_2 \tag{23}$$

$$Case\ 5 \quad f_{(6)} = \frac{sin^2\theta}{\pi A_1} \int_0^{L/2} dy_1 \int_0^{y_1 D/L} dx \int_0^{W} dy_2 \int_0^{y_2 D/L} \frac{xz}{\{(y_1-y_2)^2+x^2+z^2-2xzcos\theta\}^2} dz \tag{24}$$

$$Case\ 6 \quad f_{(7)} = \frac{sin^2\theta}{\pi A_1} \int_0^{L/2} dy_1 \int_{y_1 D/L}^{0} dx \int_0^{W} dy_2 \int_0^{y_2 D/L} \frac{xz}{\{(y_1-y_2)^2+x^2+z^2-2xzcos\theta\}^2} dz \tag{25}$$

$$Case\ 7 \quad f_{(8)} = \frac{sin^2\theta}{\pi A_1} \int_0^{L/2} dy_1 \int_{-y_1 D/L}^{0} dx \int_0^{W/2} dy_2 \int_0^{y_2 D/L} \frac{xz}{\{(y_1-y_2)^2+x^2+z^2-2xzcos\theta\}^2} dz \tag{26}$$

The analytical solutions of equations (21) to (26) are long and complex because they require the handling of Spence functions, Gamma function, sums of polylogarithms, modified Bessel functions of first species and zero, one, and two orders; for this reason, they are not presented in this study.

For the solution of equations (21) to (26), the same procedure for Case 1 is used, obtaining the following approximations to calculate the view factor for Cases 2 to 7.

$$Case\ 2 \quad f_{(3)} = 2f_{(1)} \cdot \{(-0.001Y^3 + 0.033Y^2 - 0.14Y + 0.265)\psi^2 + (0.011Y^3 - 0.177Y^2 + 0.7Y - 0.615)\psi - 0.01Y^3 + 0.142Y^2 - 0.475Y + 1.29\} \tag{27}$$

$$Case\ 3 \quad f_{(4)} = 2f_{(1)} \cdot \{(-0.031Y^3 + 0.424Y^2 - 1.257Y + 1.1)\psi^2 + (0.071Y^3 - 0.975Y^2 + 2.92Y - 2.06)\psi - 0.034Y^3 + 0.462Y^2 - 1.268Y + 1.6\} \tag{28}$$

$$Case\ 4 \quad f_{(5)} = 2f_{(1)} \cdot \{(-0.01Y^2 + 0.24Y + 0.67)\psi^2 + (0.02Y^2 - 0.31Y - 2.2)\psi - 0.02Y^2 + 0.27Y + 3\} \tag{29}$$

$$Case\ 5 \quad f_{(6)} = 2f_{(1)} \cdot \{(-0.02Y^3 + 0.29Y^2 - 1.1Y + 0.6)\psi^2 + (0.06Y^3 - 0.88Y^2 + 2.96Y - 4.41)\psi - 0.04Y^3 + 0.55Y^2 - 1.41Y + 1.87\} \tag{30}$$

$$Case\ 6 \quad f_{(7)} = 2f_{(1)} \cdot \{(-0.011Y^3 + 0.12Y^2 - 0.025Y + 0.52)\psi^2 + (0.025Y^3 - 0.307Y^2 + 0.49Y - 1.64)\psi - 0.134Y^3 + 0.183Y^2 - 0.35Y + 2.47\} \tag{31}$$

$$Case\ 7 \quad f_{(8)} = 2f_{(1)} \cdot \{(0.015^2 - 0.108Y + 0.08)\psi^2 + (-0.015Y^2 + 0.096Y + 0.048)\psi - 0.001Y^2 + 0.04Y + 0.058\} \tag{32}$$

Figure 10 plots in ±3% and ±6% error band the $D_{\%}$ obtained with equation (18) for the view factors calculated with SMR and BCR for Cases 2 to 7.

For Case 2, Figure 10 shows that BCRs have the best fit with respect to AS, with a mean error of ±3% in 97.6% of the $(Y;X)$ points analyzed. On the contrary, the view factors obtained with SMR have a lower fit with respect to AS, with mean errors of ±3% and ±6% in 28,5% and 64.3% of the $(Y;X)$ points evaluated, respectively.

For Case 3, Figure 10 shows that BCRs have a better fit with respect to AS, with mean errors of ±3% and ±6% in 92.9% and 100% of the $(Y;X)$ points analyzed. The view factors obtained with SMR have a lower fit with respect to AS, computing mean errors of ±3% and ±6% in 38.1% and 69.0% of the $(Y;X)$ points evaluated, respectively.

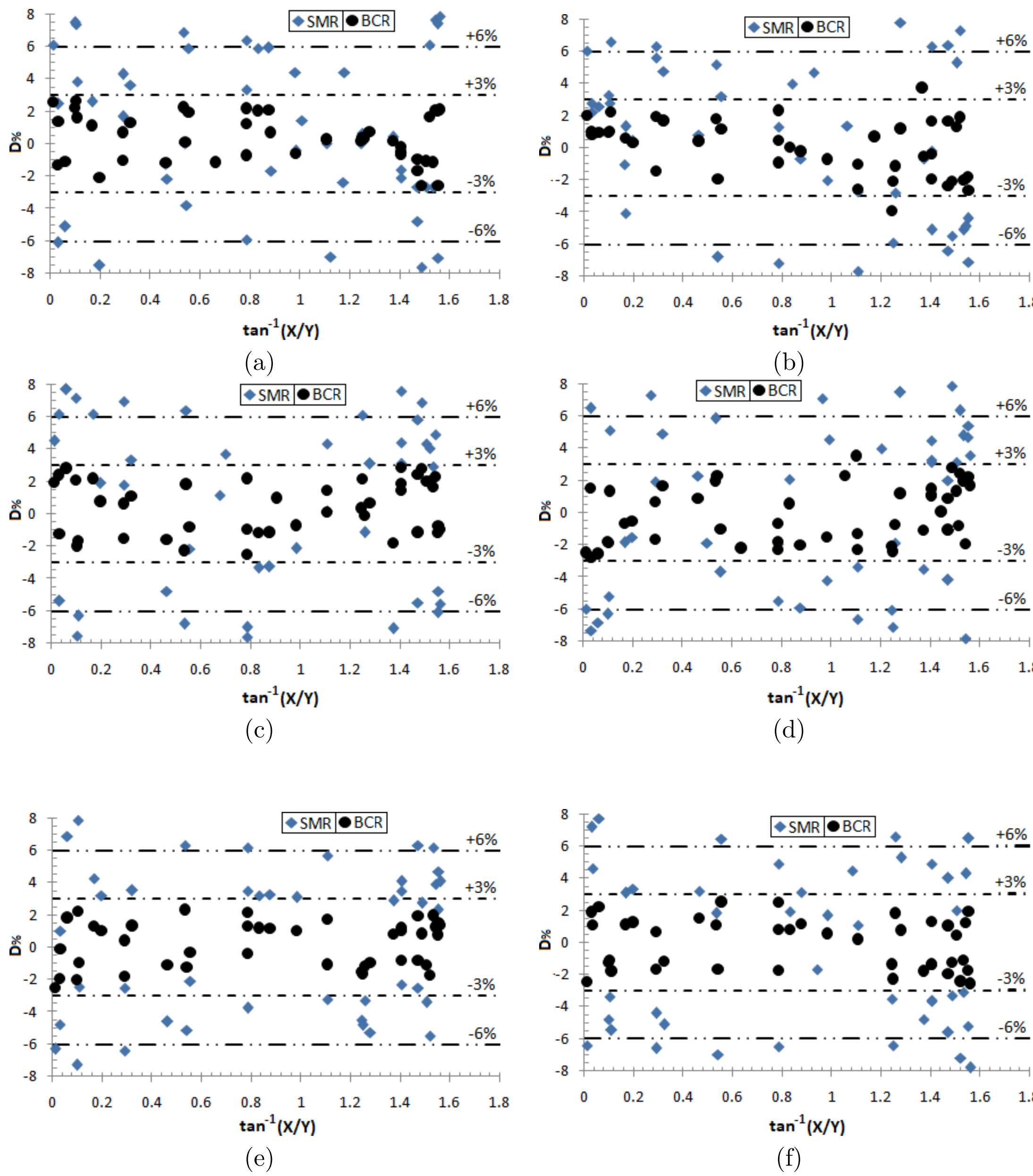

Figure 10. $D_{\%}$ values obtained with equation (18) for the cases analyzed. (a) Case 2; (b) Case 3; (c) Case 4; (d) Case 5; (e) Case 6; (f) Case 7

For Case 4, Figure 10 shows that BCRs have a better fit with respect to *AS* with mean errors of ±3% and ±6% in 90.5% and 100% of the $(Y;X)$ points analyzed. In contrast, the view factors obtained with SMR have a lower fit with respect to AS, with mean errors of ±3% and ±6% in 21.4% and 61.9% of the $(Y;X)$ points evaluated, respectively.

For Case 5, Figure 10 shows that BCRs have a better fit with respect to *AS* with mean errors of ±3% and ±6% in 95.2% and 100% of the $(Y;X)$ points analyzed. The view factors obtained with SMR have a lower fit with respect to AS, computing mean errors of ±3% and ±6% in 26.2% and 71.4% of the $(Y;X)$ points evaluated, respectively.

For Case 6, Figure 10 shows that BCRs have a better fit with respect to AS with mean errors of ±3% in 100% of the $(Y;X)$ points analyzed. On the contrary, the view factors obtained with SMR have a lower fit with respect to AS, with mean errors of ±3% and ±6% in 31.0% and 81.0% of the $(Y;X)$ points evaluated, respectively.

For Case 7, Figure 10 shows that BCRs have a better fit with respect to AS with mean errors of ±3% in 100% of the $(Y;X)$ points analyzed. The view factors obtained with SMR have a lower fit with respect to AS, computing mean errors of ±3% and ±6% in 23.8%

and 73.8% of the $(Y;X)$ points evaluated, respectively.

3.2. Other geometric configurations

In Figure 3, the emitting and receiving surfaces are divided into four triangular surfaces, resulting in $0.5n^{n-1} = 0.5 \cdot 4^{4-1} = 32$ possible combinations (see Figure 11). Using the view factors $f_{(1)}$ to $f_{(8)}$, it is possible to obtain the view factors for the remaining configurations by applying the rule of sums and the algebra of form factors. Table 5 shows the relationships for computing the view factor for the configurations in Figure 11.

Table 5. View factor settings for triangular surfaces

Case	$\mathbf{F_{(1-2)} \cdots f_{(n)}}$	Case	$\mathbf{F_{(1-2)} \cdots f_{(n)}}$
Case 8	$f_{(9)} = f_{(5)}$	Case 20	$f_{(21)} = 3f_{(3)} + f_{(8)} - 2f_{(6)} - 2f_{(7)}$
Case 9	$f_{(10)} = f_{(5)}$	Case 21	$f_{(22)} = 4f_{(1)} + 3f_{(6)} + 3f_{(7)} - 3f_{(3)} - 2f_{(4)} - 4f_{(5)} - f_{(8)}$
Case 10	$f_{(11)} = 2f_{(1)} - f_{(2)}$	Case 22	$f_{(23)} = 4f_{(5)} + f_{(3)} + f_{(8)} - 2f_{(6)} - 2f_{(7)}$
Case 11	$f_{(12)} = f_{(6)} + f_{(7)}$	Case 23	$f_{(24)} = 5f_{(3)} + 4f_{(4)} + 5f_{(5)} + f_{(8)} - 4f_{(1)} - 4f_{(2)} - 4f_{(6)} - 4f_{(7)}$
Case 12	$f_{(13)} = 2f_{(2)} - f_{(5)}$	Case 24	$f_{(25)} = 2f_{(1)} + f_{(4)} - 2f_{(2)}$
Case 13	$f_{(14)} = 4f_{(1)} + f_{(5)} - 4f_{(2)}$	Case 25	$f_{(26)} = 2f_{(1)} + f_{(3)} - 2f_{(2)}$
Case 14	$f_{(15)} = 2f_{(4)} - f_{(6)} - f_{(7)}$	Case 26	$f_{(27)} = f_{(2)} - f_{(3)}$
Case 15	$f_{(16)} = 4f_{(1)} + f_{(6)} + f_{(7)} - 2f_{(3)} - 2f_{(4)}$	Case 27	$f_{(28)} = f_{(2)} - f_{(4)}$
Case 16	$f_{(17)} = 2f_{(3)} - f_{(6)} - f_{(7)}$	Case 28	$f_{(29)} = f_{(5)} - f_{(6)} - f_{(7)}$
Case 17	$f_{(18)} = f_{(3)} + f_{(8)}$	Case 29	$f_{(30)} = 2f_{(3)} + 2f_{(4)} + f_{(5)} - 4f_{(2)} - f_{(6)} - f_{(7)}$
Case 18	$f_{(19)} = f_{(6)} + f_{(7)} - f_{(3)} - f_{(8)}$	Case 30	$f_{(31)} = 2f_{(2)} + f_{(6)} + f_{(7)} - f_{(5)} - 2f_{(4)}$
Case 19	$f_{(20)} = 4f_{(5)} + f_{(3)} + f_{(8)} - 2f_{(6)} - 2f_{(7)}$	Case 31	$f_{(32)} = 2f_{(2)} + f_{(6)} + f_{(7)} - f_{(5)} - 2f_{(3)}$

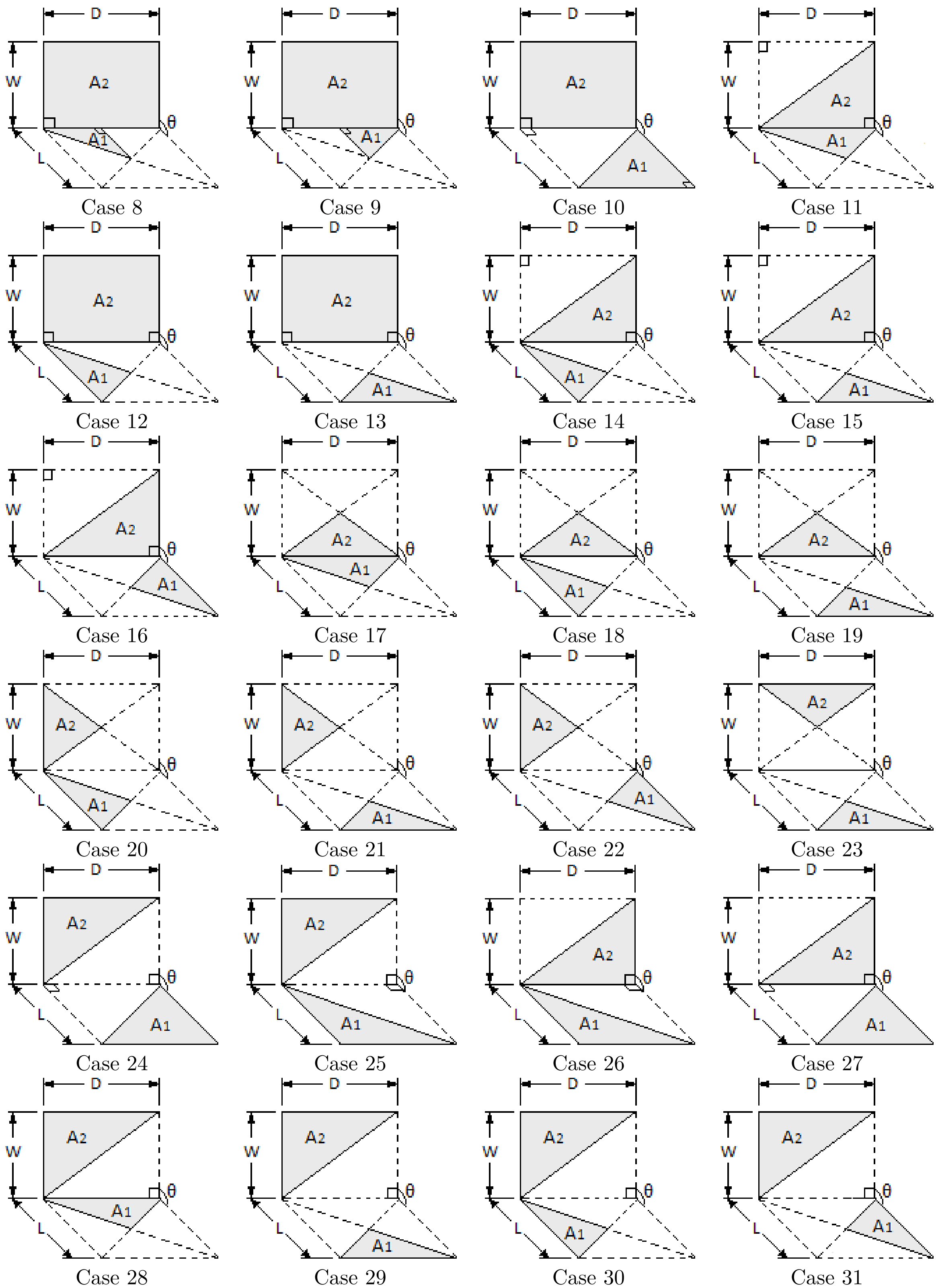

Figure 11. View factor settings for triangular surfaces

4. Conclusions

This study developed an approximate method to determine the view factor for 32 combinations of triangular geometries with common edges and angle θ included, located in a 3-D space.

To validate the proposed models, 42 examples with various aspect ratios were evaluated for each geometry of the eight basic cases, comparing the results obtained by the AS with those of the SMR with five intervals and those computed by the proposed method with BCR.

In all the cases evaluated, the RCB showed the best fits with an error of ±6% in more than 90% of the samples, and the SMR showed an average dispersion of ±6% in 65% of the data, confirming the validity of the hypothesis on its use. For the remaining 24 geometric configurations studied, the basic relations for calculating the view factor from the expressions obtained for the eight basic cases were presented.

The practical nature of the contribution and the reasonable fitting values obtained demonstrate that this proposal is a suitable tool to be applied in thermal engineering and radiation heat transfer calculation tasks.

Due to the lack of similar precedents in the literature, the proposed method highlights this research's scientific and practical value. The solutions provided could be incorporated into the available catalogs for calculating view factors.

Acknowledgments

The author gratefully acknowledges the assistance and recommendations from Professor Dr. John R. Howell, Department of Mechanical Engineering, University of Texas, Austin, and Professor Dr. Jack H. Lewis, Department of Mathematics, Massachusetts Institute of Technology, USA.

References

[1] J. R. Howell and M. P. Mengüç, "Radiative transfer configuration factor catalog: A listing of relations for common geometries," *Journal of Quantitative Spectroscopy and Radiative Transfer*, vol. 112, no. 5, pp. 910–912, 2011. [Online]. Available: https://doi.org/10.1016/j.jqsrt.2010.10.002

[2] Y. F. Nassar, "Analytical-numerical computation of view factor for several arrangements of two rectangular surfaces with non-common edge," *International Journal of Heat and Mass Transfer*, vol. 159, p. 120130, 2020. [Online]. Available: https://doi.org/10.1016/j.ijheatmasstransfer.2020.120130

[3] M. F. Modest and S. Mazumder, "Chapter 4 - View factors," in *Radiative Heat Transfer (Fourth Edition)*, fourth edition ed., M. F. Modest and S. Mazumder, Eds. Academic Press, 2022, pp. 127–159. [Online]. Available: https://doi.org/10.1016/B978-0-12-818143-0.00012-2

[4] Y. Camaraza-Medina, A. Hernández-Guerrero, and J. L. Luviano-Ortiz, "Analytical view factor solution for radiant heat transfer between two arbitrary rectangular surfaces," *Journal of Thermal Analysis and Calorimetry*, vol. 147, pp. 14 999–15 016, 2022. [Online]. Available: https://doi.org/10.1007/s10973-022-11646-4

[5] Y. Camaraza Medina, *Introducción a la termotransferencia*. Editorial Universitaria (Cuba), 2020. [Online]. Available: https://bit.ly/44PcgsO

[6] J. R. Howell, *A Catalog of Radiation Configuration Factors*. McGraw-Hill, 1982. [Online]. Available: https://bit.ly/42qHzIJ

[7] J. R. Howell, M. Pinar Menguc, and R. Siegel, *Thermal Radiation Heat Transfer*. CRC Press, 2010. [Online]. Available: https://bit.ly/42u9jfy

[8] M. K. Gupta, K. J. Bumtariya, H. Shukla, P. Patel, and Z. Khan, "Methods for evaluation of radiation view factor: A review," *Materials Today: Proceedings*, vol. 4, no. 2, Part A, pp. 1236–1243, 2017, 5th International Conference of Materials Processing and Characterization (ICMPC 2016). [Online]. Available: https://doi.org/10.1016/j.matpr.2017.01.143

[9] A. Narayanaswamy, "An analytic expression for radiation view factor between two arbitrarily oriented planar polygons," *International Journal of Heat and Mass Transfer*, vol. 91, pp. 841–847, 2015. [Online]. Available: https://doi.org/10.1016/j.ijheatmasstransfer.2015.07.131

[10] A. Narayanaswamy and P. Meyappan, "An analytic expression for radiation view factors between two planar triangles with arbitrary orientations," in *Proceedings of CHT-15. 6th International Symposium on ADVANCES IN COMPUTATIONAL HEAT TRANSFER*, 12 2015, pp. 1545–1550. [Online]. Available: https://doi.org/10.1615/ICHMT.2015.IntSympAdvComputHeatTransf.1500

[11] R. Sudharshan Reddy, D. Arepally, and A. Datta, "View factor computation and radiation energy analysis in baking oven with obstructions: Analytical and numerical method," *Journal of Food Process Engineering*, vol. 46, p. e14270, 01 2023. [Online]. Available: http://dx.doi.org/10.1111/jfpe.14270

[12] Y. Zhou, R. Duan, X. Zhu, J. Wu, J. Ma, X. Li, and Q. Wang, "An improved model to calculate radiative heat transfer in hot combustion gases," *Combustion Theory and Modelling*, vol. 24, no. 5, pp. 829–851, 2020. [Online]. Available: https://doi.org/10.1080/13647830.2020.1769866 https://doi.org/10.1080/13647830.2020.1769866

[13] X.-J. Yi, L.-Y. Zhong, T.-B. Wang, W.-X. Liu, D.-J. Zhang, T.-B. Yu, Q.-H. Liao, and N.-H. Liu, "Near-field radiative heat transfer between hyperbolic metasurfaces based on black phosphorus," *The European Physical Journal B*, vol. 92, no. 9, p. 217, Sep 2019. [Online]. Available: https://doi.org/10.1140/epjb/e2019-100274-y

[14] J. R. Ehlert and T. F. Smith, "View factors for perpendicular and parallel rectangular plates," *Journal of Thermophysics and Heat Transfer*, vol. 7, no. 1, pp. 173–175, 1993. [Online]. Available: https://doi.org/10.2514/3.11587

[15] C. K. Krishnaprakas, "View factor between inclined rectangles," *Journal of Thermophysics and Heat Transfer*, vol. 11, no. 3, pp. 480–481, 1997. [Online]. Available: https://doi.org/10.2514/2.6267

[16] H. J. Sauer Jr., "Configuration factors for radiant energy interchange with triangular areas," *ASHRAE Transactions*, vol. 80, no. 2, pp. 268–279, 1974. [Online]. Available: https://bit.ly/3I0jXm0

[17] Y. Camaraza-Medina, A. A. Sánchez Escalona, O. M. Cruz-Fonticiella, and O. F. García-Morales, "Method for heat transfer calculation on fluid flow in single-phase inside rough pipes," *Thermal Science and Engineering Progress*, vol. 14, p. 100436, 2019. [Online]. Available: https://doi.org/10.1016/j.tsep.2019.100436

[18] W. Boeke and L. Wall, "Radiative exchange factors in rectangular spaces for the determination of mean radiant temperatures," *Building services engineering*, vol. 43, pp. 244–253, 1976.

[19] F. F. Sönmez, H. Ziar, O. Isabella, and M. Zeman, "Fast and accurate ray-casting-based view factor estimation method for complex geometries," *Solar Energy Materials and Solar Cells*, vol. 200, p. 109934, 2019. [Online]. Available: https://doi.org/10.1016/j.solmat.2019.109934

[20] S. Francisco, A. Raimundo, A. Gaspar, A. V. Oliveira, and D. Quintela, "Calculation of view factors for complex geometries using Stokes' theorem," *Journal of Building Performance Simulation*, vol. 7, pp. 203–216, 05 2014. [Online]. Available: http://dx.doi.org/10.1080/19401493.2013.808266

[21] S.-A. Biehs, R. Messina, P. S. Venkataram, A. W. Rodríguez, J. C. Cuevas, and P. Ben-Abdallah, "Near-field radiative heat transfer in many-body systems," *Rev. Mod. Phys.*, vol. 93, p. 025009, Jun 2021. [Online]. Available: https://doi.org/10.1103/RevModPhys.93.025009

[22] Y. Camaraza-Medina, A. Hernández-Guerrero, and J. L. Luviano-Ortiz, "Experimental study on influence of the temperature and composition in the steels thermo physical properties for heat transfer applications," *Journal of Thermal Analysis and Calorimetry*, vol. 147, no. 21, pp. 11 805–11 821, Nov 2022. [Online]. Available: https://doi.org/10.1007/s10973-022-11410-8

[23] M. Lakhi and A. Safavinejad, "Numerical investigation of combined force convective-radiative heat transfer in a horizontal channel with Lattice Boltzmann method," *Journal of Thermal Analysis and Calorimetry*, vol. 146, no. 4, pp. 1911–1922, Nov 2021. [Online]. Available: https://doi.org/10.1007/s10973-020-10136-9

[24] M. Bonnici, P. Mollicone, M. Fenech, and M. A. Azzopardi, "Analytical and numerical models for thermal related design of a new pico-satellite," *Applied Thermal Engineering*, vol. 159, p. 113908, 2019. [Online]. Available: https://doi.org/10.1016/j.applthermaleng.2019.113908

[25] Y. Camaraza-Medina, "Methods for the determination of the heat transfer coefficient in air cooled condenser used at biomass power plants," *International Journal of Heat and Technology*, vol. 39, no. 5, pp. 1443–1450, 2021. [Online]. Available: https://doi.org/10.18280/ijht.390505